



REVIEW ARTICLE | APRIL 11 2019

Recent advances in high refractive index dielectric nanoantennas: Basics and applications

Special Collection: [2019 Nanoscience and Nanotechnology](#)A. I. Barreda; J. M. Saiz; F. González; F. Moreno ; P. Albella  

AIP Advances 9, 040701 (2019)

<https://doi.org/10.1063/1.5087402>

CrossMark

**AIP Advances**Special Topic: Machine Vision,
Optical Sensing and Measurement**Submit Today**

Recent advances in high refractive index dielectric nanoantennas: Basics and applications

Cite as: AIP Advances 9, 040701 (2019); doi: 10.1063/1.5087402

Submitted: 31 December 2018 • Accepted: 1 April 2019 •

Published Online: 11 April 2019



A. I. Barreda, J. M. Saiz, F. González, F. Moreno,^{a)} and P. Albella^{a)} 

AFFILIATIONS

Department of Applied Physics, University of Cantabria, Avda. Los Castros, s/n, 39005 Santander, Spain

^{a)}Correspondence: pablo.albella@unican.es and morenof@unican.es

ABSTRACT

Nanoparticles made of High Refractive Index dielectric materials have been proposed as an alternative to metals driven by their low-losses and magnetic response. The coherent effects between the electric and magnetic resonances are responsible for their exceptional directionality properties that make them attractive in applications where enhancing light-matter interaction and controlling the radiation direction is extremely relevant. These nanoparticles, when used as unit-cells of more complex systems, such as metasurfaces, result to be essential in the design of novel optical devices. Their low-losses, strong confinement of electromagnetic energy and the outstanding scattering efficiencies show these nanoantennas as promising candidates for Surface Enhanced Spectroscopies, non-linear phenomena or sensing. Here, we describe and discuss the origins and recent advances in this rapidly developing field of dielectric nanophotonics, paying special attention to the main significant contributions we have done since its startup to boost its progress. In particular, light directivity, steering and switching of light, spectroscopy, sensing and non-linear phenomena, third harmonic generation are some of the applications that motivated this brief overview.

© 2019 Author(s). All article content, except where otherwise noted, is licensed under a Creative Commons Attribution (CC BY) license (<http://creativecommons.org/licenses/by/4.0/>). <https://doi.org/10.1063/1.5087402>

I. INTRODUCTION

Metallic nanostructures are object of high interest due to their ability to show resonances in the optical response driven by the collective behavior of the conduction electrons near the surface of the metal, the so-called surface plasmons, that later gave name to the field of plasmonics. Plasmon resonances depend strongly on the optical properties, geometry and size of the structures, allowing for the manipulation and tuning of light at subwavelength scale. Nanostructures showing plasmon resonances can act as optical nanoantennas, providing a versatile tool to control light beyond the conventional diffraction limit.^{1,2} These enhanced light-matter interactions mediated by plasmons enabled many applications such as ultrasensitive (bio-) sensing,³ surface enhanced spectroscopies,⁴ information processing, etc.

However, plasmonic excitations are known to be affected by relatively large losses and the absence of magnetic response at optical frequencies. This unavoidable problem together with the ambition to have more control over light-matter interaction, made researchers to go beyond plasmonics.⁵ Based on the very basics

of electromagnetic theory, i.e. Mie solution for light scattering of small spheres,⁶ Kerker focused on some special conditions of the problem.⁷ He showed that it is possible to control the direction of the light scattered by *point-like* magnetodielectric particles, suppressing either the backward or the forward scattered light at certain conditions, known as Kerker conditions. This work stimulated the study of subwavelength dielectric particles with high refractive index (HRI), such as silicon or germanium subwavelength-sized spherical particles. These particles, unlike metals show electric but also magnetic mode resonances^{8–10} that provide a potential to constitute building blocks of novel photonic platforms to efficiently control the direction of light-scattering. Less than a decade ago, it was theoretically reported^{8,10,11} and experimentally demonstrated^{12,13} that subwavelength-sized HRI dielectric particles can mimic the response of Kerker's ideal magnetodielectric particles showing electric and magnetic resonances, and its coherent interference can lead to unidirectional scattering when satisfying Kerker conditions. Big efforts were devoted to explore HRI dielectric structures, to find novel efficient ways to control the directionality of light propagation in a broader sense, not just optimizing the

scattering in the forward and backward directions but also introducing the steering or switching of light.^{14–18} Different shapes like isolated spheroids,^{10,12,13,19} disks,²⁰ dimers, aggregates^{21–23} or core-shell particles^{24–29} and materials such as Si, GaP, Ge and others were explored.

The presence of these HRI dielectric nanoantennas can also be extended to more complex systems, such as metasurfaces, which are just artificial flat ultrathin optical components consisting of arrays of subwavelength optical nanoantennas.^{20,30–38} The optical effects of metasurfaces are mainly determined by the resonant properties of the constituting nanostructures. One example of this is the high transmission efficiency that a metasurface can offer when its unit cell consists of low aspect-ratio dielectric nanoantennas acting as Huygens' sources. In this case, a spectral overlap between the electric and magnetic dipolar resonances is responsible for this effect.^{20,32,39} On the other hand, perfect flat reflectors have been also reported using metasurfaces built of high aspect-ratio dielectric resonators, by achieving the spectral separation of the two resonances.^{36,37,40}

Other remarkable aspect of these dielectric nanoparticles arises from the fact that HRI dielectric nanoantennas can be a powerful alternative to their plasmonic counterparts, as an element to control the near field optical response at the nanoscale and with very low-losses. Unlike metallic antennas, where the antenna effects are produced by plasmons, dielectric particles made of HRI dielectrics rely on fields and displacement currents induced in their structure. In plasmonic nanoantennas, gold and silver are the most commonly used because of their high DC conductivities.⁴¹ However, at optical frequencies interband transitions play a detrimental role in these metals.⁴² This loss mechanism leads to Joule heating of the structure and its local environment.^{43–45} Localized heating is a strong limitation for both the design of real devices and the performance of the nanoantennas themselves.^{46,47} Local heating of the plasmonic structures changes their refractive indices via the thermo-optic effect and depending on the illuminating power, nanoantennas can even be reshaped and/or melted, thus strongly affecting their nanoscale lighting and photonic modulation capabilities.⁴⁸ To this end, exploiting the coherent interaction between the electric and magnetic dipolar resonances induced in subwavelength low-loss HRI spherical particles, it is possible to concentrate light in electric and magnetic hot-spots. This launched a new type of surface enhanced spectroscopy (Raman and Fluorescence) based on low-loss nanoantennas as it was theoretically proposed in Refs. 44 and 49 and later experimentally demonstrated in Ref. 45.

Lastly, we must highlight that HRI dielectric nanoantennas are also becoming key elements for nonlinear nano-optics, in particular for third harmonic generation (THG), which currently has applications such as commercial laser equipment by exciting bulk nonlinear crystals with large illumination powers.⁵⁰ As previously described, Si, Ge or GaP nanoantennas, at their Mie resonances, can highly enhance electric and magnetic fields within or around themselves, enabling intriguing optical effects such as the control of directional scattering. Another interesting effect for THG is the excitation of nonradiative anapole modes.^{51–53} Moreover, from the generalized Miller's rule,⁵⁴ a HRI dielectric material implies a high third-order nonlinear susceptibility medium, making the dielectric nanoantenna a key element for THG processes. Furthermore, the size of enhanced

field regions produced by Mie resonances in dielectric nanoantennas can highly exceed that corresponding to plasmonic modes in metallic nanostructures, enabling THG from relatively large volumes, boosting the nonlinear effect.⁵³

After this introduction about how HRI dielectric nanoantennas, emerged as an alternative to plasmonic units for the design of different nanophotonic devices, we continue this brief overview with a discussion of the contribution we have made to the field in different topics. These will be grouped in three different sections. 1) Light directivity, steering and switching, focused on the discussion of different HRI structures and the study of different scattering properties to control light directionality. 2) Spectroscopy and sensing, where the first part is devoted to review the use of dimer-like HRI-based single nanoantennas to produce both high surface enhanced fluorescence and surface enhanced Raman scattering, while generating a negligible temperature increase in their hot spots and surrounding environments. The second concerns the use of the intriguing scattering properties of single HRI dielectric structures, such as the magnetic resonances, as a novel way to sense the refractive index of the surrounding medium and the presence of impurities on the material. 3) In this final section, some of the recent applications where HRI dielectric nanoantennas played a significant role in nonlinear optics and metasurfaces, are discussed. Concerning non-linear optics, we review a key concept for the realization of highly efficient nonlinear optical systems at nanometer scales, which is the combination of plasmonic nanostructures with resonant HRI dielectric nanoparticles to enhance their field confinement capabilities. Furthermore, this section shows that the optimum emission wavelength can be tuned from the blue to the red region of the visible spectrum. To finish this part, we discuss a recent demonstration of how HRI dielectric metasurfaces when conveniently designed can act as a switch from high transmission to high reflection by simply changing the linear polarization state of light in the NIR region.

II. DIRECTIVITY AND SWITCHING

In 1983, Kerker et al. described some unusual electromagnetic scattering effects for magnetic spheres much smaller than the wavelength of the incident radiation.⁷ Under the so-called Kerker conditions, the response of a particle to an electromagnetic incident radiation can be described in terms of two crossed induced dipoles, one electric and one magnetic, of equal amplitude. When $\epsilon = \mu$, both dipoles oscillate in-phase⁵⁵ (the first electric and magnetic Mie coefficients a_1, b_1 verify $a_1 = b_1$). For this case the radiation is scattered in the forward region and the backward scattered intensity ($\theta = 180^\circ$) is zero. It is known as the First Kerker condition or Zero-Backward condition. The opposite behavior, null scattered intensity in the forward direction (Zero-Forward condition), should be observed whenever ϵ and μ verify

$$\epsilon = \frac{4 - \mu}{2\mu + 1} \quad (1)$$

In this case, ($a_1 = -b_1$) and the electric and magnetic dipoles oscillate out-of-phase. According to the optical theorem, which establishes that the extinction cross section is proportional to the scattering amplitude in the forward direction $S(0^\circ)$, see Eq. (2),⁵⁶ the scattered intensity in the forward direction cannot be null.⁵⁷

$$C_{ext} = \frac{4\pi}{k^2} \text{Re}(S(0^\circ)) \quad (2)$$

k being the wave vector of the incident radiation.

For Eq. (2) to be satisfied in a zero-forward regime, C_{ext} should be zero. However, for non-absorbing materials (the imaginary part of their dielectric constant is null), absorption cross section is zero, while the scattering cross section is not (the scattered intensity has important values in other directions different to forward). This means that C_{ext} is different from zero and the Zero-Forward condition is inconsistent with the optical theorem.⁵⁷ Alù and Engheta in Ref. 58 demonstrated that Kerker theory is valid in the quasistatic limit (where the size of the particle is considerably smaller than the wavelength of the incident radiation in vacuum), without violating the optical theorem, when the radiative correction is taken into account. When this correction is included, the scattered intensity in the forward direction is very small compared to other scattering angles but it is not identically zero. This condition is known as near Zero-Forward condition or Second Kerker condition.

In Ref. 57, Kerker conditions were revisited and corrected expressions were proposed to satisfy the optical theorem in the Zero-Backward and near Zero-Forward conditions, taking into account the radiative correction. Although the Zero-Backward condition is the same than that proposed by Kerker, a new expression was found for the near Zero-Forward condition, in which the magnitude of the correction depends on the size of the scatterer.

These electromagnetic scattering features were predicted some decades ago, but only recently (2012) have been verified experimentally, the reason being the absence of natural magnetic media at optical frequencies, and the lossy character of magnetic materials in the microwave regime. However, HRI dielectric materials like silicon^{8,59,10} show strong magnetic and electric dipolar resonances in the visible, as well as in telecom and near-infrared frequencies, where absorption is negligible for silicon. Similar effects can be observed for other semiconductor materials.^{60,44,61}

The first experimental verification of Kerker conditions with a single HRI dielectric sphere was carried out in the microwave range

(see Fig. 1)¹² by taking advantage of the scalability of Maxwell's equations. Notice that the electromagnetic response of a system is the same at any spectral range if the ratio $\lambda/(na)$ is kept constant, being λ the wavelength of the incident radiation, n the refractive index of the particle and a its radius. This means that the experiments carried out in Ref. 12 are comparable to those of a Si sphere in the near-infrared¹⁰ if the material used satisfies the scale factor $\lambda/(na)$. Not long after that, both conditions were demonstrated in the VIS.¹³

The asymmetric character of the scattering is also noticed in the polarization of the scattered electromagnetic wave. In order to see this, it is helpful to use a polarimetric parameter, i.e. the degree of linear polarization of the scattering at a right-angle configuration, $P_L(\theta)$ for $\theta = 90^\circ$ ($P_L(90^\circ)$):

$$P_L(\theta) = \frac{I_s(\theta) - I_p(\theta)}{I_s(\theta) + I_p(\theta)} \quad (3)$$

where I_s and I_p correspond to the scattered intensity when the incident radiation is linearly polarized perpendicular and parallel to the scattering plane, respectively.

Under the dipolar approximation (particles scatter as electric or magnetic dipoles), it is possible to obtain a simplified expression for the linear polarization degree at right angle scattering configuration $P_L(90^\circ)$:

$$P_L(90^\circ) = \frac{|a_1|^2 - |b_1|^2}{|a_1|^2 + |b_1|^2} \quad (4)$$

From the above equation, it can be inferred that if the particle behaves as an electric (magnetic) dipole, $P_L(90^\circ) = 1$ ($P_L(90^\circ) = -1$). This suggests that the polarimetric parameter $P_L(90^\circ)$ can provide information about the electric or magnetic character of the resonances.⁶²⁻⁶⁴ Due to the implications of the Kerker conditions in the dipolar regime ($|a_1| = |b_1|$), the linear polarization degree at right-angle scattering is zero, $P_L(90^\circ) = 0$, at the wavelengths where such conditions are fulfilled. For larger particles, higher order terms should be included in the expansion of the fields. Assuming that only the dipolar and quadrupolar contributions are significant, $P_L(90^\circ)$ takes the following expressions,⁶²

$$P_L(90^\circ) = \frac{9|a_1|^2 + 25|b_2|^2 + 30\text{Re}\{b_1 a_2^*\} - 9|a_1|^2 - 25|b_2|^2 - 30\text{Re}\{a_1 b_2^*\}}{9|a_1|^2 + 25|b_2|^2 + 30\text{Re}\{b_1 a_2^*\} + 9|a_1|^2 + 25|b_2|^2 + 30\text{Re}\{a_1 b_2^*\}} \quad (5)$$

a_2 and b_2 correspond to the quadrupolar electric and magnetic Mie coefficients, respectively. Re refers to the real part of a complex number and the asterisk denotes the complex conjugate. $P_L(90^\circ)$ deviates from 1 or -1 due to the presence of quadrupolar electric or magnetic contributions, respectively. From Eq. (5) it can be concluded that $P_L(90^\circ)$ can also be useful for determining the charge distributions (dipolar or quadrupolar, in this case) apart from their electric or magnetic nature. In addition, $P_L(90^\circ)$ may provide information about both the NP size and the refractive index of the surrounding medium (scattering coefficients are related to the particle size

and the relative refractive index).⁶⁵ In the case of working with aggregates of particles (dimers, as an example), $P_L(90^\circ)$ is a suitable parameter to identify the interaction between the resonant modes of the constituent NPs, as well as its orientation and position.⁶² The directionality properties of this kind of NPs can be enhanced by taking advantage of the coherent effects produced not only between dipolar contributions but also between these and high-order modes, giving rise to anomalous scattering effects.^{66,67}

Several geometries have been considered in order to produce both efficient excitation and spectral overlapping of dipolar

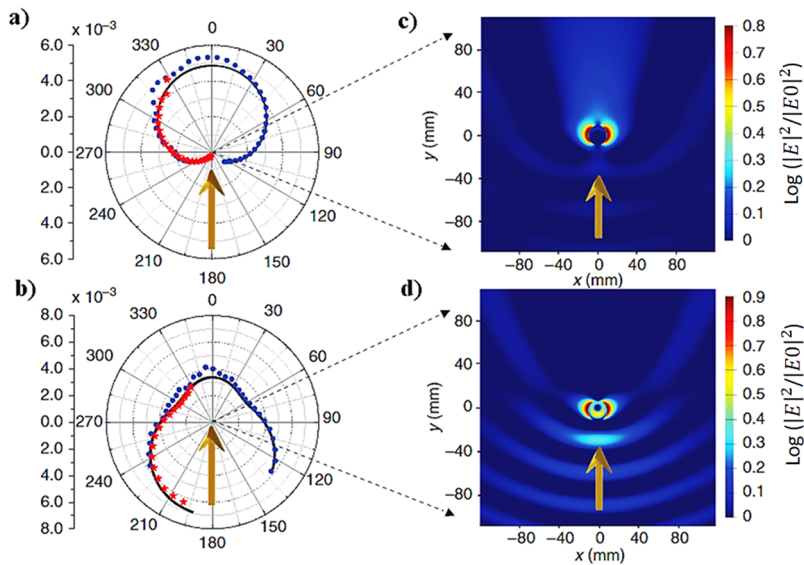


FIG. 1. Scattered intensity in far-field by a sphere of radius $R = 9$ mm and electric permittivity $\epsilon_1 = 16.5$ at the a) Zero-Backward ($\lambda = 84$ mm) and b) near Zero-Forward ($\lambda = 69$ mm) conditions. Experimental values are represented by blue circles and red stars. Theoretical curves are represented by black solid lines. Total near-field intensity distribution maps (logarithmic scale) at the c) Zero-Backward and d) near Zero-Forward conditions. Brown arrows represent in a) and b) are the direction of the incident radiation and the color bar used in c) and d) corresponds to a rainbow template where blue and red are the min and max values, respectively.¹² Reproduced with permission from Geffrin *et al.*, Nature communications 3, 1171 (2012). Copyright 2012 Springer Nature.

or higher order electric or magnetic resonances. In Ref. 20, it was shown that it is possible to tune both, the dipolar electric and magnetic resonances, to reach a maximum overlap of both resonances. This was done by tailoring the aspect ratio of silicon nanodisks, but other geometries, like metallo-dielectric or all-dielectric core-shell NPs, and aggregates (mainly dimers), have been studied with the same objective.^{22,24–26,28,68}

In particular, in Ref. 22 we demonstrated that an asymmetric dimer of silicon HRI dielectric NPs can provide unidirectional forward scattering with high efficiency when the dimer configuration satisfies the First Kerker condition at the resonant peaks of electric and magnetic dipolar modes. In Fig. 2a, the spectral dependence of the scattering cross sections (forward and backward directions) are shown, together with the Forward/Backward (F/B) ratio,

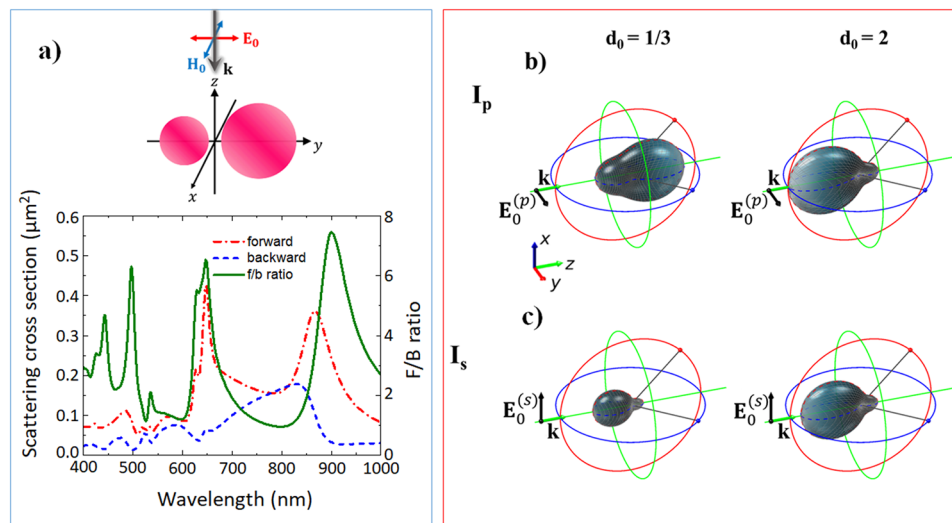


FIG. 2. (a) Spectral dependence of the scattering cross sections in the forward and backward directions, together with the Forward/Backward (F/B) ratio for a dimer of two Si spheres of diameter $D_1 = 165$ nm and $D_2 = 225$ nm separated by a 5 nm gap. Top: scheme of the nanoantenna configuration and excitation used in the calculation. The dimer was illuminated by a plane wave polarized parallel to the dimer axis.²² Reproduced with permission from Shibnuma *et al.*, Nanoscale 8, 14184–14192 (2016). Copyright 2016 Royal Society of Chemistry. (b-c) 3D scattering directivity diagrams at the near Zero-Forward condition wavelength ($\lambda = 67$ nm). The radii of the particles are $R_1 = R_2 = 9$ nm and their dielectric permittivity is $\epsilon_1 = \epsilon_2 = 15.7 \pm 0.3$. (b) The structure is illuminated with a plane wave propagating along the z -axis (\mathbf{k}) and linearly polarized parallel to the y -axis, $\mathbf{E}_0^{(p)}$ (longitudinal configuration). (c): polarization perpendicular to the y -axis, $\mathbf{E}_0^{(s)}$ (transverse configuration). Left column: Strong interaction between the dimer components ($d_0 = 1/3$). Right column: Weak interaction between both particles of the dimer ($d_0 = 2$).²³ Reproduced with permission from Barreda *et al.*, Scientific Reports 8, 7976 (2018). Copyright 2018 Springer Nature.

for a dimer of two silicon spheres of diameters $D_1 = 165$ nm and $D_2 = 225$ nm separated by a gap distance of 5 nm. The configuration used in the calculation is shown in the inset. Our experiments, using a silicon nanodisk dimer on a transparent substrate, confirmed the high efficiency of the unidirectional forward scattering.²² The results might be of application in fields like solar cells or lighting instruments.

With the objective of observing broadband unidirectional forward scattering, we proposed to use a symmetric dimer of spherical particles.^{23,69} The particles radii were $R_1 = R_2 = R = 9$ nm and with a dielectric permittivity of $\epsilon_1 = \epsilon_2 = 15.7 + 0.3i$. This particle size was chosen so that the experiments could be carried out in the microwave region, same as in Ref. 10. In particular, we evidenced that, it is possible to find, in the dipolar regime, two spectral regions where the incident radiation is forward-scattered. They correspond to the Zero-Backward condition and to a new “near Zero-Backward” condition. The origin of the last one, which is a 180° “rotated” version of the near Zero-Forward condition, resides in the strong interaction effects between the particles. For that reason, it can only be observed when the distance between the particles is small, and the structure is illuminated by a plane wave linearly polarized parallel to the axis that joins both particles. In particular, a Fano-like resonance (originated by the interference between both the sharp magnetic and the broad electric dipolar modes) gives rise to this new Scattering Directionality Condition (SDC). In Figs. 2b–c, we show the scattering diagrams at frequencies where the near Zero-Forward condition holds. The diagrams correspond to the two incident polarizations, along the axis of the dimer (E_p) in Fig. 2b and perpendicular to the axis of the dimer (E_s) in Fig. 2c. For the purpose of taking into account the interaction effects, we defined the parameter $d_0 = d/R$, where d is the distance between both components of the dimer and R is their radius. We explored two extreme cases, $d_0 = 1/3$ (strong interaction) and $d_0 = 2$ (weak interaction). It can be observed how, in the case of strong interaction and excited with I_p , a rotation of the scattering pattern is manifested from a near Zero-Forward to a novel “near Zero-Backward” condition.

Dimer configurations have also been demonstrated to be useful for redirecting the incident radiation respect to the traditional forward and backward directions. This effect has implications for building switching devices. For the symmetric dimer case whose components are close enough to interact in a controlled way, we showed that the scattered intensity at 90° can be null or maximum by depending on the polarization of a single frequency excitation.^{14,70} Interestingly, this behavior transforms the dimer into a two-output switching unit (or beam-splitter element) whose binary state depends only on the polarization of the exciting radiation. This possibility was also proposed with a dark field microscope configuration, but right-angle scattering seems to be more suitable for the practical purpose of building operational optical circuits.²¹ The most important advantage of the proposed system with respect to the former ones is that the “off” state corresponds to null values of the scattered intensity. As the particle interaction increases one of the natural resonances (the dipolar magnetic) of the isolated particle spectrally evolves to an asymmetric shape resonance (Fano-like): this can be considered the origin of the switching effect. This behavior can be observed in Fig. 3, where we show the spectral evolution of the scattered intensity at 90° for longitudinal (I_p) and transverse polarizations (I_s) of the incident radiation. We also plot the behavior of the linear polarization degree at 90° , $P_L(90^\circ)$. The analysis is carried out for two different distances between the particles, $d_0 = 2$ (see Fig. 3a, weak interaction effects between the particles) and $d_0 = 1/3$ (see Fig. 3b, strong interaction effects).

By means of these asymmetric dimers we evidenced first theoretically¹⁵ and later experimentally,¹⁷ that beam steering effects can be achieved by just changing the frequency of the incident radiation. This mechanism is based on the tuning of the interference between the electric and magnetic dipoles that are excited in each of the nanoparticles, that is, electric-electric, magnetic-magnetic and electric-magnetic dipole interactions. In Fig. 4a, we show the far-field radiation patterns of the scattered light at $\lambda = 500$ nm and $\lambda = 630$ nm for an asymmetric silicon dimer of spherical particles

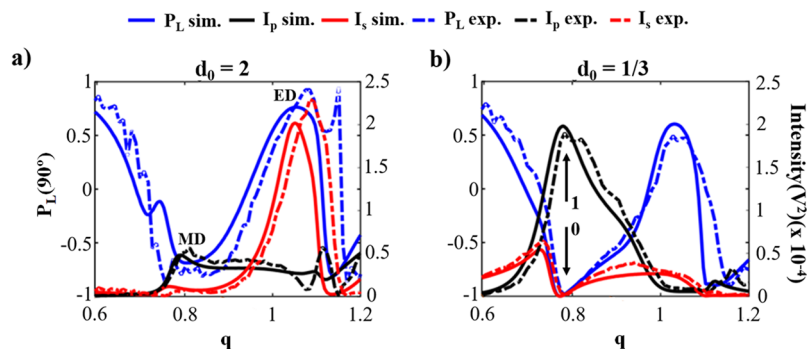


FIG. 3. Far-field scattered intensity at 90° and linear polarization degree at right angle scattering configuration ($P_L(90^\circ)$) for a HRI dielectric dimer of spherical particles as a function of the size parameter q ($q = 2\pi R/\lambda$). Particles radii $R_1 = R_2 = 9$ nm and dielectric permittivity $\epsilon_1 = \epsilon_2 = 15.7 + 0.3i$. The distance between both components of the dimer is $d = 18$ nm ($d_0 = 2$) and $d = 3$ nm ($d_0 = 1/3$). It is illuminated by a plane wave linearly polarized parallel (I_p) or perpendicular (I_s) to the scattering plane. (a) Simulation and measurement for $d_0 = 2$. (b) Simulation and measurements for $d_0 = 1/3$. (MD = Magnetic dipole resonance, ED = Electric dipole resonance). Simulations (solid line). Measurements (dash line). $P_L(90^\circ)$ blue line. I_s (red line). I_p (black line). The low and high states are indicated with the 0 and 1 arrows respectively.¹⁴ Reproduced with permission from Barreda *et al.*, Nature Communications 8, 13910 (2017). Copyright 2017 Springer Nature.

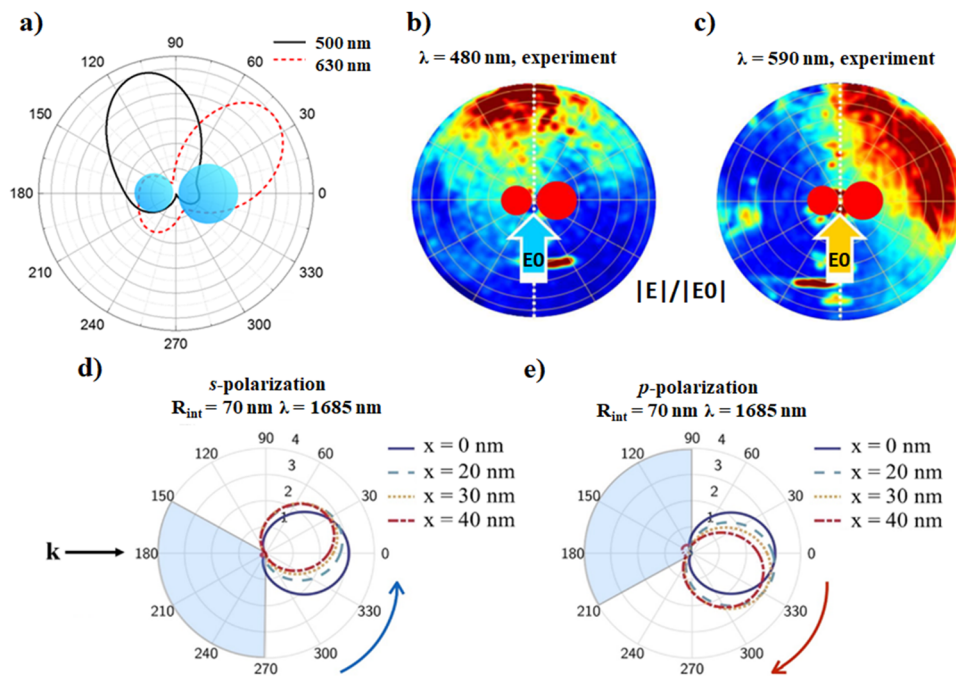


FIG. 4. a) Theoretical light scattering polar plot at $\lambda = 500$ nm and $\lambda = 630$ nm for an asymmetric silicon dimer of spherical particles of radii $R_1 = 75$ nm and $R_2 = 115$ nm, separated by a gap of $d = 8$ nm.¹⁵ Top-right: normalized experimental scattering patterns for silicon disks of height $H = 170$ nm, diameters $D_1 = 180$ nm, $D_2 = 250$ nm and gap $d = 40$ nm at $\lambda = 480$ nm (b) and $\lambda = 590$ nm (c).¹⁷ Reproduced with permission from Shibamura *et al.*, ACS Photonics **4**, 489 (2017). Copyright 2017 American Chemical Society. The color map corresponds to a rainbow template where blue and red are the min and max values, respectively. Bottom row: scattered intensity diagrams for an Ag-Si metallo-HRI dielectric core-shell NP (particle radius $R_{ext} = 230$ nm, core radius $R_{int} = 70$ nm) as a function of the core displacement for polarizations of the incident radiation (d) perpendicular (s-incident polarization) (I_s) and (e) parallel (p-incident polarization) (I_p) to the scattering plane. Different core shifts along the x-axis: 0 nm (blue solid line), 20 nm (blue dashed line), 30 nm (yellow dotted line) and 40 nm (red dash-dotted line), are represented. The black arrow labelled with k indicates the propagation direction of the incident beam. The blue and red arrows refer to the rotation direction.¹⁶ Reproduced with permission from Barreda *et al.*, Scientific Reports **7**, 11189 (2017). Copyright 2017 Springer Nature.

of radii $R_1 = 75$ nm and $R_2 = 115$ nm, separated by a gap of $d = 8$ nm. This effect was demonstrated by an experiment carried out on silicon disks of height $H = 170$ nm, diameters $D_1 = 180$ nm, $D_2 = 250$ nm and gap $d = 40$ nm (see Figs. 4b–c).

Similar effects were manifested through eccentric metallo-dielectric core-shell NPs.^{16,71} We demonstrated that the incident radiation can be scattered into some specific directions respect to that of forward or backward by means of Ag-Si core-shell structures, when the core is shifted respect to the center of the NP. In this case, the rotation of the scattering pattern only depends on the polarization of the incident radiation, instead of the frequency (see Figs. 4d–e). Other important difference with respect to the dimer configuration is that only one particle is required. Attending to the directionality properties of these scattering units, chains of them were built, evidencing good radiation guiding effects.

III. SPECTROSCOPY AND SENSING

The above applications are based on far-field coherent effects between electric and magnetic resonances giving rise to interesting directionality properties. However, for developing new spectroscopic tools, it is necessary to pay attention to near-field properties.

In particular, field enhancement in the proximity of the particle surface is required. In analogy to plasmonic aggregates, constituted by two or more metallic NPs, ensembles of dielectric particles exhibit large enhancements of the electromagnetic energy in the gap (hot-spots). Because of the low absorption of HRI dielectric NPs the temperature increase in the hot-spots is negligible, while they still allow to design nanoantennas with both high Surface Enhanced Fluorescence and Surface Enhanced Raman Scattering. An example of this is shown in Ref. 49, where we demonstrated that electric and magnetic hotspots can be observed in the gap of silicon dimers. In particular, we explored the possibility of designing effective antennas based on these dielectric nanoparticles, and produce enhancements of the fluorescence of single emitters such as molecules or quantum dots located in their vicinity. When placing dipolar emitters in the gap, the decay rate of the emitter is modified because of the environment due to the Purcell effect. It was shown that silicon nanoantennas present larger and more stable quantum efficiencies than plasmonic dimers in the VIS and NIR spectral regions, due to their lack of ohmic losses. In Fig. 5a, it is shown the electric near-field enhancement calculated for a dimer of radius 150 nm and dimer gap 4 nm at $\lambda = 1100$ nm for incident electric field polarized along the dimer axis. In Fig. 5b, magnetic near-field

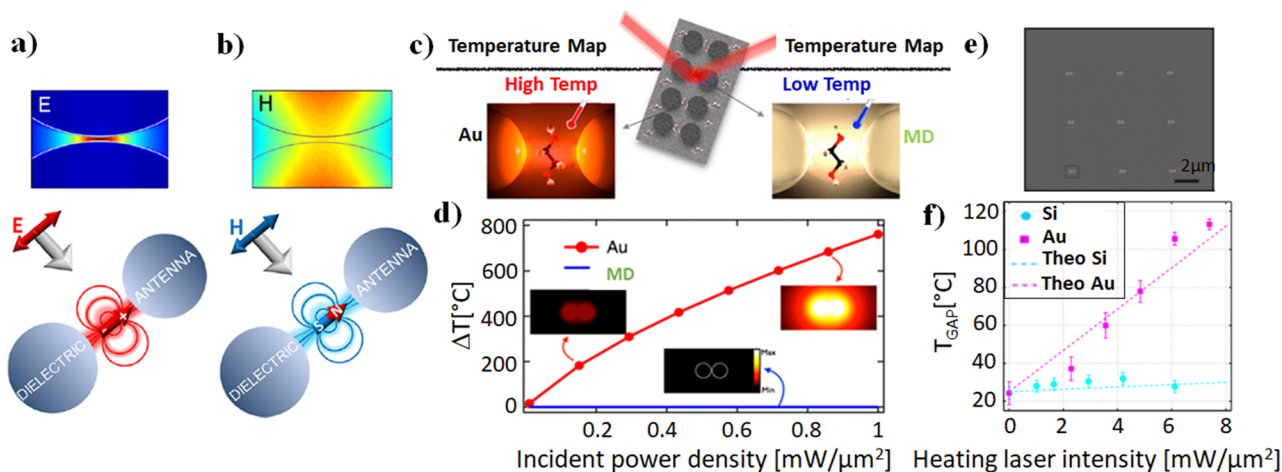


FIG. 5. (a) Electric near-field enhancement (E/E_{inc}) calculated for a dimer of radius 150 nm and dimer gap 4 nm at $\lambda = 1100$ nm for incident electric field polarized along the dimer axis. The field distribution clearly shows the localization of the enhanced electric field in the dimer gap.⁴⁹ (b) Magnetic near-field enhancements calculated for the same system as in (a) for incident magnetic field polarized along the dimer axis (s-polarized). This configuration helps to extract the enhanced magnetic field to the dimer gap.⁴⁹ (c) Artistic impression of a molecule located in the centre of a metallic dimer made of gold (left) and a dielectric dimer made of GaP (right). (d) Temperature difference in the centre of a spheres dimer calculated at the absorption resonance of Au as a function of the incident power density, for both Au and GaP in the VIS range. The radii of the Au and GaP spheres correspond to 50 nm and 100 nm, respectively. The gap is 10 nm. The insets show the temperature distribution around the spheres dimer for selected incident power densities.⁴⁴ (e) SEM image of the array of nanostructures fabricated in Si on a silicon-on-insulator substrate. Each nanoantenna consists of two identical disks with a diameter of 220 nm, a height of 200 nm and a 20 nm gap in between. Scale bar, 2 μ m. (f) Extracted temperature in the gap for selected silicon (cyan) and gold (magenta) nanoantennas as a function of the heating laser intensity at 860 nm. The gold disks diameter and height are 140 nm and 40 nm, respectively. The gap between the particles is 20 nm, like for the silicon dimer. The dashed lines show the numerical calculations for the temperature at the gap, presenting good agreement with the experimental data.⁴⁵ (a, b), (c, d) and (e, f) Reproduced with permission from Albella *et al.*, *J. Phys. Chem. C*, **117**, 13573–13584 (2013). Copyright 2013 American Chemical Society; Albella *et al.*, *ACS Photonics* **1**, 524–529 (2014). Copyright 2014 American Chemical Society; and Caldarola *et al.*, *Nat. Commun.* **6**, 7915 (2015). Copyright 2015 Springer Nature respectively.

enhancement calculated for the same system as in Fig. 5a for incident magnetic field polarized along the dimer axis (s-polarized) is represented.

Heat studies were conducted in Ref. 44, where, by using HRI dielectric NPs instead of plasmonics, heat dissipation is avoided, while an evidence of near-field concentration and enhancement (hot-spots) is still present (see Fig. 5c). In particular, we analyzed the temperature in the center of the gap of a sphere dimer at the absorption resonance of Au as a function of the incident power density for both Au and GaP in the VIS range (see Fig. 5d). The radii of the Au and GaP spheres are 50 nm and 100 nm, respectively. The gap is 10 nm. Due to the inherent ohmic losses of metallic nanostructures, a local heating of the NP is produced. This aspect, often neglected, is the cause of an increase in the NP temperature, and the surrounding medium, which can induce changes in the optical properties of the medium and the NP itself, disrupting the response of the system. This drawback is not observed for the case of HRI dielectric NPs. Due to their negligible absorption in VIS and NIR, incident radiation can propagate through the NP without being absorbed. This effect was shown experimentally by means of silicon and gold nanoantennas (see Fig. 5e, where a SEM image of the array of nanostructures fabricated in Si on a silicon-on-insulator substrate is shown). It is worthy to note that, manufacturing pure GaP disks on a low refractive index material was very challenging at that time, therefore the experimental demonstration was carried out by means of silicon

disks. The local temperature around Si and Au nanoantennas was compared in Ref. 45. As expected, when increasing the heating laser intensity the temperature increase in the gap is ultra-low for the Si nanoantennas, while it exceeds 80 °C for the gold nanoantennas, see Fig. 5f.

Due to the low-losses, HRI dielectric NPs have also been proposed as an alternative to the metallic ones for sensing applications. Resonances of HRI dielectric materials are redshifted and weakened as the refractive index of the surrounding medium (m_{med}) increases.⁶⁰ This suggests that extinction efficiency (Q_{ext}) of HRI dielectric NPs can work as a sensor of changes in the refractive index of the surrounding medium. Although Q_{ext} can be easily analyzed by means of numerical simulations, its experimental measurement (in VIS-NIR) is complicated. This motivated a search of other parameters that could be measured in a more direct way, therefore showing as an alternative for sensing applications. We proposed to use the spectral evolution of $P_L(90^\circ)$ as a polarimetric parameter for sensing, providing an estimate of m_{med} . Right-angle measurements have the advantage of avoiding parasitic effects due to the incident radiation. In Ref. 65, isolated spherical NPs of radius $R = 200$ nm were used to check their potential as sensors of the refractive index of the surrounding medium. Particles were made of representative HRI dielectric materials and m_{med} was varied in the interval $m_{med} \in [1, 2]$. In order to evaluate the accuracy of $P_L(90^\circ)$ as an estimator of m_{med} , it is necessary to analyze the positions of the resonances as a

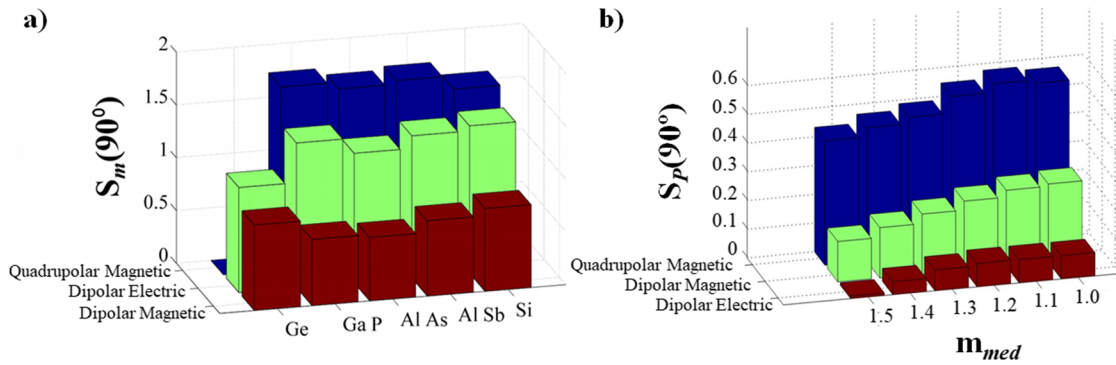


FIG. 6. (a) Sensitivity of the linear polarization degree, $S_p(90^\circ)$ to m_{med} (with $m_{med} \in [1, 2]$) at the resonance wavelengths for the selected materials.⁶⁵ (b) $S_p(90^\circ)$ to NP purity where the percent Si ranges from 100% to 98.98% for different surrounding media, whose refractive indices $m_{med} \in [1, 1.5]$.⁷⁴ For both figures particle radius corresponds to $R = 200$ nm. (a) and (b) Reproduced with permission from Barreda *et al.*, Optics Express **23**, 9157 (2015). Copyright 2015 OSA and Barreda *et al.*, Journal of Quantitative Spectroscopy and Radiative Transfer **162**, 190 (2015). Copyright 2015 Elsevier, respectively.

function of the wavelength at which they occur λ_{res} , i.e., $\frac{\delta P_L(90^\circ)}{\delta \lambda} = 0$. A parameter, $S_m(90^\circ)$, was introduced in order to obtain the sensitivity of $P_L(90^\circ)$ to m_{med} :

$$S_m(90^\circ) = \left| \left(\frac{\delta P_L(90^\circ)}{\delta m_{med}} \right)_{\lambda_{res}} \right| \quad (6)$$

This parameter is expressed in inverse refractive index units (RIU^{-1})⁷² and can be used to assess the influence of m_{med} variations on the values of $P_L(90^\circ)$. Figure 6a shows $S_m(90^\circ)$ values for different semiconductors at λ_{res} , averaged over the range $m_{med} \in [1, 2]$. Most of the $S_m(90^\circ)$ values are larger than 0.5 RIU^{-1} for both dipolar electric and magnetic resonances, as can be seen in Figure 6a, and increase toward 1.5 RIU^{-1} for the quadrupolar magnetic resonance. Notice that $S_m(90^\circ)$ values of the order of 1.0 RIU^{-1} imply similar changes in both $P_L(90^\circ)$ and in m_{med} .

Most studies consider that the HRI dielectric material of which NPs are made, is 100% pure. It means that impurities are not considered. However, this is not a realistic assumption from an experimental point of view. In the case of Si NPs, the most common impurities are Aluminium (Al), Titanium (Ti) and Iron (Fe). In Ref. 73 the influence of the purity grade of a silicon NP on the extinction and absorption efficiency spectra was studied. Later, we analyzed the evolution of $P_L(90^\circ)$ as a function of the purity of spherical Si NPs of radius $R = 200$ nm embedded in different dielectric media.⁷⁴ To consider using the linear polarization degree $P_L(90^\circ)$ to measure NP purity, we focused on the evolution of the three resonances observed in the spectrum, the dipolar electric and the dipolar and quadrupolar magnetic resonances. We obtained the value of the linear polarization $P_L(90^\circ)$, for the different purity grades, at the wavelengths where the resonances appear, λ_{res} . The sensitivity of $P_L(90^\circ)$ to the purity of the sample can be obtained through the following parameter, $S_p(90^\circ)$

$$S_p(90^\circ) = \left| \left(\frac{\delta P_L(90^\circ)}{\delta \text{Purity}(\%)} \right)_{\lambda_{res}} \right| \quad (7)$$

Several values of $S_p(90^\circ)$ are shown in Fig. 6b, where it can be noticed how, as the refractive index of the surrounding medium increases,

the sensitivity decreases. Magnetic resonances exhibit the highest sensitivities, reaching values up to near 0.6.

We would like to finish this section by pointing out that most of the studies of HRI dielectric materials have been explored at either optical or near IR frequencies. However, we recently showed that some materials, when nanostructured, show special properties in the UV, like enhanced field efficiency, low dissipation losses and heat generation, and versatile options to reach scattering directionality.⁷⁵ Some examples are aluminum nitride, aluminum arsenide, aluminum phosphide, diamond, titanium dioxide and cerium dioxide. We studied their performance, when forming either isolated nanoparticles or dimers, to build nanoantennas and unit cells for more complex metasurfaces.⁷⁵ The interest of such structures lies on potential applications where photocatalytic or biosensing processes need to be optimized by reducing ohmic losses.

IV. OTHER APPLICATIONS: NON-LINEAR EFFECTS AND METASURFACES

Directionality properties exhibited by HRI dielectric structures make them attractive for many different applications. To name a few, sensing,^{65,76} radiation guiding at the nanoscale (nanoantennas),^{27,15,17,77} waveguiding,⁷⁸ Fano resonances^{21,79–81} or building optical devices⁶⁶ for enhancing nonlinear phenomena (like second and third harmonic generation).^{52,53,82–84} Concerning the later, the possibility of exciting anapole modes has been demonstrated to be efficient for boosting a nonlinear response. This is because of the large confinements of the electromagnetic radiation inside the NP. In Ref. 53, we showed that the nonlinear response from a HRI nanoantenna can be significantly improved by adding a metallic element in order to obtain a metal-dielectric hybrid nanostructure. In particular, the plasmonic resonance of a gold nanoring can boost the anapole mode supported by a Si nanodisk, enhancing the electric field inside the large third-order susceptibility dielectric. Furthermore, the third harmonic emission can be tuned throughout the optical regime by geometrically modifying the hybrid nanoantenna. In Fig. 7a–b, the schematic of the experimental configuration is shown, together with the SEM image of the hybrid nanoantenna

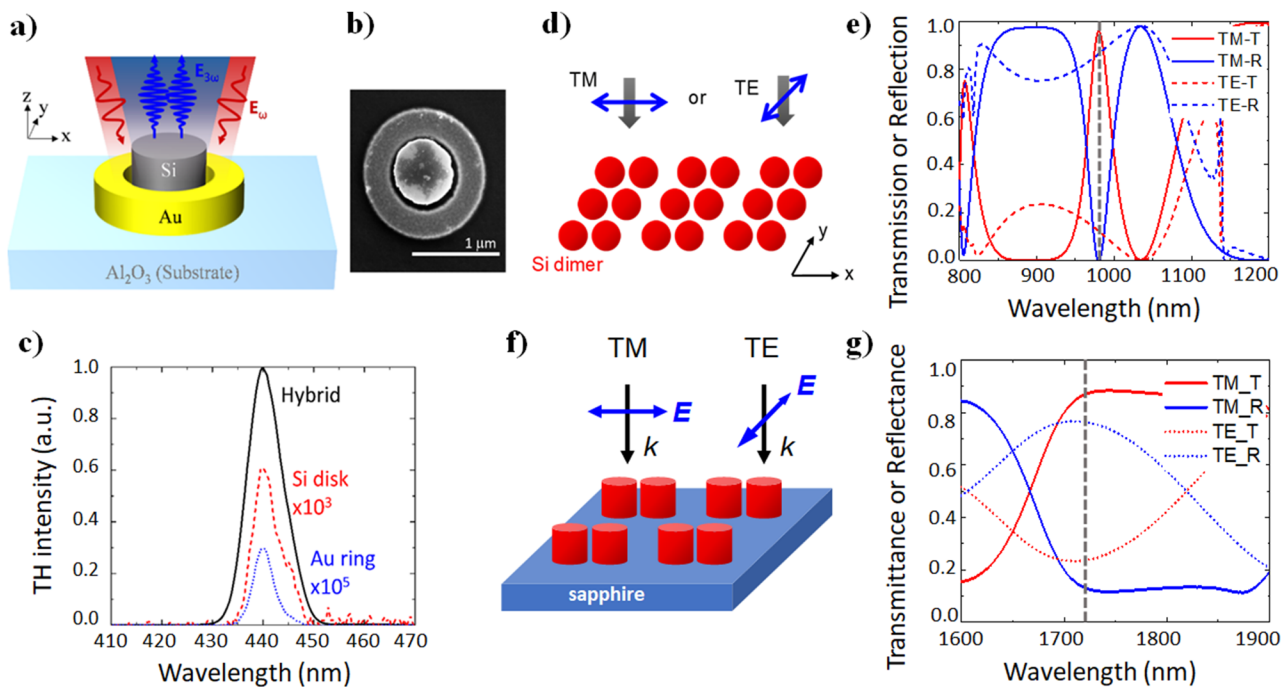


FIG. 7. (a) Schematic of the experimental configuration used for third harmonic generation studies. The Si nanodisk has a diameter $D_1 = 680$ nm with height $H_1 = 155$ nm, and the Au nanoring has an inner diameter $D_{21} = 780$ nm, outer diameter $D_{22} = 1360$ nm and height $H_2 = 80$ nm. The gap corresponds to 50 nm. The structure is located on a sapphire substrate.⁵³ (b) SEM image of the fabricated hybrid nanoantenna. The scale bar is 1 μ m. (c) Third harmonic generation spectra of the hybrid structure, isolated Si nanodisk and bare Au nanoring measured at $\lambda = 1320$ nm excitation wavelength and 1 μ W excitation power. (d) Schematic image of a Si sphere dimer array in air illuminated by a linearly polarized incident light. The diameter of the spheres correspond to 300 nm and separation distance is 10 nm. The periodicities of the array along (x) and perpendicular (y) to the dimer axis were set to 790 nm and 480 nm, respectively. (e) Transmission (red lines) and reflection (blue lines) spectra of the Si sphere dimer array under the illumination of TM (solid lines) and TE (broken lines) polarization. (f) Schematic image of a Si disk dimer array on a sapphire substrate illuminated by linearly polarized incident light. The diameter and height of the Si nanodisks are 652 nm and 314 nm, respectively with a gap of 50 nm. The periodicities of the array were set to 1544 nm and 852 nm along and perpendicular to the dimer axis, respectively. (g) Experimental Transmission (red lines) and reflection (blue lines) spectra of the Si disk dimer array illuminated with TM (solid lines) and TE (broken lines) polarized plane wave.³⁷ (a, b, c) and (d, e, f, g) Reproduced with permission from Shibamura *et al.*, Nano Letters **17**, 2647 (2017). Copyright 2017 American Chemical Society and Shibamura *et al.*, Applied Physics Letters **112**, 063103 (2018). Copyright 2018 AIP Publishing LLC respectively.

used to enhance the third harmonic generation.⁵³ Figure 7c shows the result –third harmonic spectra– of exciting the hybrid nanoantenna and its individual (isolated) components at $\lambda = 1320$ nm, i.e. at the valley of the extinction spectrum (excitation of the anapole mode), where the electric field inside the dielectric is predicted to be maximum. A single peak at $\lambda = 440$ nm $= (1320 \text{ nm})/3$ was observed in all cases, as numerically predicted. It is worth remarking that the hybrid structure exhibits a third harmonic intensity that is much larger than those of the isolated Si nanodisk and bare Au nanoring, 1.6×10^3 and 3×10^5 times respectively, demonstrating in this way the interaction between its composing parts.

HRI dielectric NPs have also been proposed as building blocks for metamaterials and metasurfaces.^{30,31} In Refs. 20, 32, 33, the directionality capabilities of single HRI dielectric NPs (in particular, the Zero-Backward condition) were exploited for designing Huygens' metasurfaces. In Ref. 34, a metasurface consisting of a uniform array of silicon nanodisks was devised for obtaining near-unity broadband transmission at visible wavelengths. Metasurfaces constituted by all-dielectric materials have also been suggested for producing

the opposite effect, i.e. enhanced reflection.³⁶ In Ref. 37, we demonstrated theoretically and experimentally, that an array of HRI dielectric nanodimers, could behave as a high transmission or reflection metasurface by changing the polarization of the incident radiation. In Fig. 7d, a schematic image of the Si dimer array in air illuminated by the linearly polarized incident light is represented. The diameter of the spheres is 300 nm and the separation, 10 nm. The periodicities of the array along (x) and perpendicular (y) to the dimer axis were set to 790 nm and 480 nm, respectively. In Fig. 7e, it is shown the transmission (red lines) and reflection (blue lines) spectra of the Si dimer array under TM (solid lines) and TE (broken lines) polarized illumination, numerically obtained by means of Finite-Difference Time-Domain (FDTD). The experiment was carried out on silicon disks (see Figs. 7f–g).

Furthermore, the possibility of building electric and magnetic mirrors has been evidenced.^{36,38,85} In particular, in Ref. 36 we showed theoretically and experimentally how an all-dielectric magnetic mirror can be produced in the terahertz band, by constructing a metasurface made of an array of silicon cube resonators.

These can simultaneously support electric and magnetic dipolar Mie resonances, and the interference between these modes can be controlled.

V. CONCLUSIONS

In this review, we have provided with a brief overview of the origins and the recent advances in the emerging field of dielectric nanophotonics paying special attention to the main significant contributions we have done since its startup and to boost its progress. In particular, the use of dielectrics instead of metals to enhance and control light-matter interaction is rapidly developing and showing a great potential in applications like light directivity, beam steering and switching, spectroscopy and sensing, metasurfaces and non-linear optics, such as third harmonic generation.

Since the discovery of the Kerker conditions, big efforts were made to find optimal structures that could enhance the Zero-Backward and near Zero-Forward conditions. We demonstrated that asymmetric dimers of spheres or disks can provide unidirectional forward scattering with high efficiency due to the achievement of the First Kerker condition at the resonant peaks of electric and magnetic dipolar modes. This is useful for lighting instruments and solar cells. Photovoltaic devices require broadband response in the NIR spectral region. Following this objective, we showed that by means of symmetric spherical dimers, it is possible to find two spectral regions (in the range, where the dipolar approximation holds) where the incident radiation is forward scattered. They correspond to the traditional Zero-Backward condition and a new “near Zero-Backward” one, being the latter caused by the interaction effects between the particles. In addition, this kind of structures, symmetric and asymmetric dimers, can be useful for redirecting the incident radiation into different directions to those of forward or backward, which is useful for beam steering and building switching devices. Similar effects can be achieved through eccentric metallo-dielectric core-shell nanoparticles.

On the other hand, nanoantennas made of HRI dielectric materials have shown to be of particular interest as an alternative to plasmonic nanoantennas in applications where light-matter interaction needs to happen with ultra-low light-into-heat conversion and high scattering efficiency, like in the case of surface enhanced spectroscopies (Raman or fluorescence). Local heating of plasmonic nanoantennas change their refractive indices via the thermo-optic effect and also, depending on the illuminating power, the heat generated by the nanoantennas can vapourize the surrounding liquid/solvent media or affect nanoemitters, molecules and proteins close to them. To circumvent the issues of losses and heating, the use of non-plasmonic materials, HRI dielectrics in our case, evidenced that silicon dimers acting as nanoantennas present larger and more stable quantum efficiencies than plasmonic ones. In addition, HRI dielectric nanostructures not only have great potential as sensors, but also as tools to determine the purity of its composition. These two last applications were demonstrated by means of the changes observed in the $P_L(90^\circ)$ spectra, at the electric and magnetic resonance wavelengths, as a function of the refractive index of the surrounding medium or the purity of the material of which NPs are made.

These nanostructures have shown useful as scattering units for building metasurfaces. In particular, we proposed two different

configurations. On the one hand, we evidenced that an array of HRI dielectric nanodimers could behave as a high transmission or reflection metasurface by changing the polarization of the incident radiation. On the other hand, we showed how a metasurface, constituted by an array of silicon cube resonators is able to work as a magnetic mirror in THz.

HRI dielectric materials are also emerging in the field of non-linear optics where they play a significant role driven by the presence of electric and magnetic modes that can lead to the recently introduced anapole mode. This mode can boost the non-linear response in nanostructures. Following this idea, we demonstrated that combining metals and HRI dielectric materials to build a single metal-dielectric hybrid nanostructure did significantly improve the THG efficiency. Furthermore, by modifying the geometrical parameters of the hybrid nanoantenna, the third harmonic emission can be tuned throughout the optical regime.

Further progress of this field is expected, some examples are: i) in some cases, backward scattering is preferable to forward scattering. Therefore, other nanoantenna geometries can be designed in order to exploit not only dipolar but also higher-order resonances. The interference including higher order modes has more parameters that can be controlled than the interference of only dipolar resonances, showing a potential to achieve the Kerker-type unidirectional backward scattering with high efficiency. ii) Non-linear effects could be enhanced by exploring other materials to form the hybrid metal-dielectric structure we reviewed here. For instance, replacing Au by other material that may show lower absorption in visible light region, possibly reducing the energy losses at the third harmonic wavelength. Also, Si could be replaced by other semiconductors, like Ge which has been reported to exhibit high third harmonic efficiency even with a single nanoscale object due to its large refractive index and third order susceptibility.

ACKNOWLEDGMENTS

This research has been supported by the Army Research Laboratory under Cooperative Agreement Number W911NF-17-2-0023 and by SODERCAN (Sociedad para el Desarrollo de Cantabria) through the Research Vicerrectorate of the University of Cantabria. P.A acknowledges funding from the Ramon y Cajal Fellowship RYC-2016-20831 and A.I.B. wants to thank the University of Cantabria for her FPU grant.

REFERENCES

- ¹ S. A. Maier, *Plasmonics—Fundamentals and Applications* (Springer, 2007).
- ² P. Bharadwaj, B. Deutsch, and L. Novotny, “Optical antennas,” *Adv. Opt. Photon* 438–483 (2009).
- ³ R. de la Rica and M. Stevens, “Plasmonic ELISA for the ultrasensitive detection of disease biomarkers with the naked eye,” *Nat Nanotechnol* 7(12), 821–4 (2012).
- ⁴ P. L. Stiles, J. A. Dieringer, N. C. Shah, and R. P. V. Duyne, “Surface-enhanced Raman spectroscopy,” *Annu. Rev. Anal. Chem.* 1, 601–626 (2008).
- ⁵ A. I. Kuznetsov, A. E. Miroshnichenko, M. L. Brongersma, Y. S. Kivshar, and B. Luk'yanchuk, “Optically resonant dielectric nanostructures,” *Science* 354(6314), aag2472 (2016).
- ⁶ G. Mie, “Beiträge zur optik trüber medien, speziell kolloidaler metallösungen,” *Annalen der Physik* 330(3), 377–445 (1906).
- ⁷ M. Kerker, D. Wang, and C. L. Giles, “Electromagnetic scattering by magnetic spheres,” *J. Opt. Soc. Am.* 3(73), 765–767 (1983).

- ⁸A. B. Evlyukhin, C. Reinhardt, A. Seidel, B. S. Luk'yanchuk, and B. N. Chichkov, "Optical response features of Si-nanoparticle arrays," *Phys Rev B* **82**, 045404 (2010).
- ⁹R. Gómez-Medina, B. García-Cámara, I. Suárez-Lacalle, F. González, F. Moreno, M. Nieto-Vesperinas, and J. J. Sáenz, "Electric and magnetic dipolar response of germanium nanospheres: Interference effects, scattering anisotropy, and optical forces," *J. Nanophotonics* **5**, 053512 (2011).
- ¹⁰A. García-Etxarri, R. Gómez-Medina, L. S. Froufe-Pérez, C. López, L. Chantada, F. Scheffold, J. Aizpurua, M. Nieto-Vesperinas, and J. J. Sáenz, "Strong magnetic response of submicron silicon particles in the infrared," *Opt. Express* **19**, 4815–4826 (2011).
- ¹¹B. Rolly, B. Stout, and N. Bonod, "Boosting the directivity of optical antennas with magnetic and electric dipolar resonant particles," *Optics Express* **20**(18), 20376–20386 (2012).
- ¹²J. M. Geffrin, B. García-Cámara, R. Gómez-Medina, P. Albella, L. S. Froufe-Pérez, C. Eyraud, A. Litman, R. Vaillon, F. González, M. Nieto-Vesperinas, J. J. Sáenz, and F. Moreno, "Magnetic and electric coherence in forward and back-scattered electromagnetic waves by a single dielectric subwavelength sphere," *Nature Communications* **3**, 1171 (2012).
- ¹³Y. H. Fu, A. I. Kuznetsov, A. E. Miroshnichenko, Y. F. Yu, and B. Luk'yanchuk, "Directional visible light scattering by silicon nanoparticles," *Nature Communications* **4**, 1527 (2013).
- ¹⁴A. I. Barreda, H. Saleh, A. Litman, F. González, J. Geffrin, and F. Moreno, "Electromagnetic polarization-controlled perfect switching effect with high-refractive-index dimers and the beam-splitter configuration," *Nature Communications* **8**, 13910 (2017).
- ¹⁵P. Albella, T. Shibanuma, and S. A. Maier, "Switchable directional scattering of electromagnetic radiation with subwavelength asymmetric silicon dimers," *Sci. Rep.* **5**, 18322 (2015).
- ¹⁶A. I. Barreda, Y. Gutiérrez, J. M. Sanz, F. González, and F. Moreno, "Light guiding and switching using eccentric core-shell geometries," *Scientific Reports* **7**, 11189 (2017).
- ¹⁷T. Shibanuma, T. Matsui, T. Roschuk, J. Wojcik, P. Mascher, P. Albella, and S. A. Maier, "Experimental demonstration of tunable directional scattering of visible light from all-dielectric asymmetric dimers," *ACS Photonics* **4**, 489 (2017).
- ¹⁸D. G. Baranov, S. V. Makarov, A. E. Krasnok, P. A. Belov, and A. Alù, "Tuning of near- and far-field properties of all-dielectric dimer nanoantennas via ultrafast electron-hole plasma photoexcitation," *Laser & Photonics Reviews* **10**(6), 1009–1015 (2016).
- ¹⁹B. S. Luk'yanchuk, N. V. Voshchinnikov, R. Paniagua-Domínguez, and A. I. Kuznetsov, "Optimum forward light scattering by spherical and spheroidal dielectric nanoparticles with high refractive index," *ACS Photonics* **2**(7), 993–999 (2015).
- ²⁰I. Staude, A. E. Miroshnichenko, M. Decker, N. T. Fofang, S. Liu, E. Gonzales, J. Dominguez, T. S. Luk, D. N. Neshev, I. Brener, and Y. Kivshar, "Tailoring directional scattering through magnetic and electric resonances in subwavelength silicon nanodisks," *ACS Nano* **7**, 7824 (2013).
- ²¹J. Yan, P. Liu, Z. Lin, H. Wang, H. Chen, C. Wang, and G. Yang, "Directional Fano resonance in a silicon nanosphere dimer," *ACS Nano* **9**, 2968 (2015).
- ²²T. Shibanuma, P. Albella, and S. A. Maier, "Unidirectional light scattering with high efficiency at optical frequencies based on low-loss dielectric nanoantennas," *Nanoscale* **8**, 14184–14192 (2016).
- ²³A. I. Barreda, H. Saleh, A. Litman, F. González, J. Geffrin, and F. Moreno, "On the scattering directionality of a dielectric particle dimer of high refractive index," *Scientific Reports* **8**, 7976 (2018).
- ²⁴W. Liu, J. Zhang, B. Lei, H. Ma, W. Xie, and H. Hu, "Ultra-directional forward scattering by individual core-shell nanoparticles," *Optics Express* **22**, 16178 (2014).
- ²⁵Y. Tsuchimoto, T. Yano, T. Hayashi, and M. Hara, "Fano resonant all-dielectric core/shell nanoparticles with ultrahigh scattering directionality in the visible region," *Optics Express* **24**, 14451 (2016).
- ²⁶R. R. Naraghi, S. Sukhov, and A. Dogariu, "Directional control of scattering by all-dielectric core-shell spheres," *Optics Letters* **40**, 585 (2015).
- ²⁷J. Li, N. Verellen, D. Vercruysse, T. Bearda, L. Lagae, and P. V. Dorpe, "All-dielectric antenna wavelength router with bidirectional scattering of visible light," *Nano Letters* **16**, 4396 (2016).
- ²⁸R. S. Savelev, O. N. Sergaeva, D. G. Baranov, A. E. Krasnok, and A. Alu, "Dynamically reconfigurable metal-semiconductor Yagi-Uda nanoantenna," *Physical Review B* **95**, 235409 (2017).
- ²⁹A. I. Barreda, Y. Gutiérrez, J. M. Sanz, F. González, and F. Moreno, "Polarimetric response of magnetodielectric core-shell nanoparticles: An analysis of scattering directionality and sensing," *Nanotechnology* **27**, 234002 (2016).
- ³⁰R. Paniagua-Domínguez, F. López-Tejeda, R. Marqués, and J. A. Sánchez-Gil, "Metallo-dielectric core-shell nanospheres as building blocks for optical three-dimensional isotropic negative-index metamaterials," *New Journal of Physics* **13**, 123017 (2011).
- ³¹S. B. Glybovski, S. A. Tretyakov, P. A. Belov, Y. S. Kivshar, and C. R. Simovski, "Metasurfaces: From microwaves to visible," *Physics Reports* **634**, 1 (2016).
- ³²S. Campione, L. I. Basilio, L. K. Warne, and M. B. Sinclair, "Tailoring dielectric resonator geometries for directional scattering and Huygens' metasurfaces," *Optics Express* **23**, 2293 (2015).
- ³³K. E. Chong, L. Wang, I. Staude, A. R. James, J. Dominguez, S. Liu, G. S. Subramania, M. Decker, D. N. Neshev, I. Brener, and Y. S. Kivshar, "Efficient polarization-insensitive complex wavefront control using Huygens' metasurfaces based on dielectric resonant meta-atoms," *ACS Photonics* **3**, 514 (2016).
- ³⁴Y. F. Yu, A. Y. Zhu, R. Paniagua-Domínguez, Y. H. Fu, B. Luk'yanchuk, and A. I. Kuznetsov, "High-transmission dielectric metasurface with 2π phase control at visible wavelengths," *Laser & Photonics Reviews* **9**, 412 (2015).
- ³⁵J. F. Algorri, B. García-Cámara, A. Cuadrado, J. M. Sánchez-Pena, and R. Vergaz, "Selective dielectric metasurfaces based on directional conditions of silicon nanopillars," *Nanomaterials* **7**, 1 (2017).
- ³⁶Z. Ma, S. M. Hanham, P. Albella, B. Ng, H. T. Lu, Y. Gong, S. A. Maier, and M. Hong, "Terahertz all-dielectric magnetic mirror metasurfaces," *ACS Photonics* **3**, 1010 (2016).
- ³⁷T. Shibanuma, S. A. Maier, and P. Albella, "Polarization control of high transmission/reflection switching by all-dielectric metasurfaces," *Applied Physics Letters* **112**, 063103 (2018).
- ³⁸P. Moitra, B. A. Slovick, W. Li, I. I. Kravchenko, D. P. Briggs, S. Krishnamurthy, and J. Valentine, "Large-scale all-dielectric metamaterial perfect reflectors," *ACS Photonics* **2**, 692 (2015).
- ³⁹K. E. Chong, B. Hopkins, I. Staude, A. E. Miroshnichenko, J. Dominguez, M. Decker, D. N. Neshev, I. Brener, and Y. S. Kivshar, "Observation of Fano resonances in all-dielectric nanoparticle oligomers," *Small* **10**, 1985 (2014).
- ⁴⁰M. Decker, I. Staude, M. Falkner, J. Dominguez, D. N. Neshev, I. Brener, T. Pertsch, and Y. S. Kivshar, "High-efficiency dielectric Huygens' surfaces," *Adv. Optical Mater.* **3**, 813–820 (2015).
- ⁴¹H. A. Atwater and A. Polman, "Plasmonics for improved photovoltaic devices," *Nat. Mater.* **9**, 205–213 (2010).
- ⁴²P. B. Johnson and R. W. Christy, "Optical constants of the noble metals," *Phys. Rev. B* **6**, 4370–4379 (1972).
- ⁴³G. Baffou and R. Quidant, "Thermo-plasmonics: Using metallic nanostructures as nano-sources of heat," *Laser Photon. Rev.* **7**, 171–187 (2013).
- ⁴⁴P. Albella, R. A. de la Osa, F. Moreno, and S. A. Maier, "Electric and magnetic field enhancement with ultralow heat radiation dielectric nanoantennas: Considerations for surface-enhanced spectroscopies," *ACS Photonics* **1**, 524–529 (2014).
- ⁴⁵M. Caldarola, P. Albella, E. Cortes, M. Rahmani, T. Roschuk, G. Grinblat, R. F. Oulton, A. V. Bragas, and S. A. Maier, "Non-plasmonic nanoantennas for surface enhanced spectroscopies with ultra-low heat conversion," *Nat. Commun.* **6**, 7915 (2015).
- ⁴⁶Z. Ioffe, T. Shamai, A. Ophir, G. Noy, I. Yutsis, K. Kfir, O. Cheshnovsky, and Y. Selzer, "Detection of heating in current-carrying molecular junctions by Raman scattering," *Nature Nanotechnology* **3**, 727–732 (2008).
- ⁴⁷D. R. Ward, D. A. Corley, J. M. Tour, and D. Natelson, "Vibrational and electronic heating in nanoscale junctions," *Nature Nanotechnology* **6**, 33–38 (2011).

- ⁴⁸A. Kuhlicke, S. Schietinger, C. Matyssek, K. Busch, and O. Benson, "In situ observation of plasmon tuning in a single gold nanoparticle during controlled melting," *Nano Lett* **13**, 2041–2046 (2013).
- ⁴⁹P. Albella, M. A. Poyli, M. K. Schmidt, S. A. Maier, F. Moreno, J. J. Sáenz, and J. Aizpurua, "Low-loss electric and magnetic field-enhanced spectroscopy with subwavelength silicon dimers," *J. Phys. Chem. C* **117**, 13573–13584 (2013).
- ⁵⁰P. A. Franken, A. E. Hill, C. W. Peters, and G. Weinreich, "Generation of optical harmonics," *Phys. Rev. Lett.* **7**, 118 (1961).
- ⁵¹A. E. Miroshnichenko, A. B. Evlyukhin, Y. F. Yu, R. M. Bakker, A. Chipouline, A. I. Kuznetsov, B. Luk'yanchuk, B. N. Chichkov, and Y. S. Kivshar, "Nonradiating anapole modes in dielectric nanoparticles," *Nature Communications* **6**, 8069 (2015).
- ⁵²G. Grinblat, Y. Li, M. P. Nielsen, R. F. Oulton, and S. A. Maier, "Enhanced third harmonic generation in single germanium nanodisks excited at the anapole mode," *Nano Letters* **16**, 4635 (2016).
- ⁵³T. Shibanuma, G. Grinblat, P. Albella, and S. A. Maier, "Efficient third harmonic generation from metal-dielectric hybrid nanoantennas," *Nano Letters* **17**, 2647 (2017).
- ⁵⁴R. W. Boyd, *Nonlinear Optics*, Academic Press, New York, 2008.
- ⁵⁵A. D. Yaghjian, "Increasing the supergain of electrically small antennas using metamaterials," *Proceedings of 3rd European Conference on Antennas and Propagation*, p. 858, 2009.
- ⁵⁶C. F. Bohren and D. R. Huffman, *Absorption and Scattering of Light by Small Particles* (John Wiley & Sons, Inc., New York, 1983).
- ⁵⁷B. García-Cámara, R. A. d. l. Osa, J. M. Saiz, F. González, and F. Moreno, "Directionality in scattering by nanoparticles: Kerker's null-scattering conditions revisited," *Optics Letters* **36**, 728 (2011).
- ⁵⁸A. Alù and N. Engheta, "How does zero forward-scattering in magnetodielectric nanoparticles comply with the optical theorem?," *Journal of Nanophotonics* **4**, 041590 (2010).
- ⁵⁹M. Nieto-Vesperinas, R. Gómez-Medina, and J. J. Sáenz, "Angle-suppressed scattering and optical forces on submicrometer dielectric particles," *J. Opt. Soc. Am. A* **28**, 54–60 (2011).
- ⁶⁰B. García-Cámara, R. Gómez-Medina, J. J. Sáenz, and B. Sepúlveda, "Sensing with magnetic dipolar resonances in semiconductor nanospheres," *Optics Express* **21**, 23007 (2013).
- ⁶¹S. Person, M. Jain, Z. Lapin, J. J. Sáenz, G. Wicks, and L. Novotny, "Demonstration of zero optical backscattering from single nanoparticles," *Nano Lett.* **13**(4), 1806–180 (2013).
- ⁶²B. Setién, P. Albella, J. M. Saiz, F. González, and F. Moreno, "Spectral behavior of the linear polarization degree at right-angle scattering configuration for nanoparticle systems," *New Journal of Physics* **12**, 103031 (2010).
- ⁶³P. Albella, J. M. Saiz, J. M. Sanz, F. González, and F. Moreno, "Nanoscale surface inspection by analyzing the linear polarization degree of the scattered light," *Optics Letters* **34**(12), 1906–1908 (2009).
- ⁶⁴B. García-Cámara, F. González, and F. Moreno, "Linear polarization degree for detecting magnetic properties of small particles," *Opt. Lett.* **35**, 4084–4086 (2010).
- ⁶⁵A. I. Barreda, J. M. Sanz, and F. González, "Using linear polarization for sensing and sizing dielectric nanoparticles," *Optics Express* **23**, 9157 (2015).
- ⁶⁶M. I. Tribelsky, J. Geffrin, A. Litman, C. Eyraud, and F. Moreno, "Small dielectric spheres with high refractive index as new multifunctional elements for optical devices," *Scientific Reports* **5**, 12288 (2015).
- ⁶⁷W. Liu and Y. S. Kivshar, "Generalized Kerker effects in nanophotonics and meta-optics," *Optics Express* **26**, 13085 (2018).
- ⁶⁸Y. Li, M. Wan, W. Wu, Z. Chen, P. Zhan, and Z. Wang, "Broadband zero-backward and near-zero-forward scattering by metallo-dielectric core-shell nanoparticles," *Scientific Reports* **5**, 12491 (2015).
- ⁶⁹A. I. Barreda, H. Saleh, A. Litman, F. González, J. Geffrin, and F. Moreno, "Scattering directionality of high refractive index dielectric particles: A note for solar energy harvesting," *Proceedings of SPIE 10527* (2018).
- ⁷⁰A. I. Barreda, H. Saleh, A. Litman, F. González, F. Moreno, and J. Geffrin, "Sphere dimers of high refractive index dielectric particles as elementary units for building optical switching devices," *11th International Congress on Engineered Materials*, 2017.
- ⁷¹A. I. Barreda, Y. Gutiérrez, J. M. Sanz, F. González, and F. Moreno, "Eccentric metallo-dielectric core-shell nanoparticles for switching and guiding purposes," *12th International Congress on Artificial Materials for Novel Wave Phenomena (Metamaterials)*, 2018.
- ⁷²Y. Xia and N. J. Halas, "Shape-controlled synthesis and surface plasmonic properties of metallic nanostructures," *MRS Bulletin* **30**, 338 (2005).
- ⁷³J. M. Sanz, R. A. d. l. Osa, A. I. Barreda, J. M. Saiz, F. González, and F. Moreno, "Influence of pollutants in the magneto-dielectric response of silicon nanoparticles," *Optics Letters* **39**, 3142 (2014).
- ⁷⁴A. I. Barreda, J. M. Sanz, R. A. d. l. Osa, J. M. Saiz, F. Moreno, F. González, and G. Videen, "Using linear polarization to monitor nanoparticle purity," *Journal of Quantitative Spectroscopy and Radiative Transfer* **162**, 190 (2015).
- ⁷⁵Y. Gutiérrez, D. Ortiz, J. M. Saiz, F. González, P. Albella, and F. Moreno, "The quest for low loss high refractive index dielectric materials for UV photonic applications," *Appl. Sci.* **8**(11), 2065 (2018).
- ⁷⁶A. I. Barreda, J. M. Sanz, R. A. d. l. Osa, J. M. Saiz, F. Moreno, F. González, and G. Videen, "Using linear polarization for sensing and monitoring nanoparticle purity," *Proceedings of SPIE 9899* (2016).
- ⁷⁷A. E. Krasnok, A. E. Miroshnichenko, P. A. Belov, and Y. S. Kivshar, "Huygens optical elements and Yagi-Uda nanoantennas based on dielectric nanoparticles," *JETP Letters* **94**, 593 (2011).
- ⁷⁸R. M. Bakker, Y. F. Yu, R. Paniagua-Domínguez, B. Luk'yanchuk, and A. I. Kuznetsov, "Resonant light guiding along a chain of silicon nanoparticles," *Nano Letters* **17**, 3458 (2017).
- ⁷⁹B. Hopkins, D. S. Filonov, A. E. Miroshnichenko, F. Monticone, A. Alù, and Y. S. Kivshar, "Interplay of magnetic responses in all-dielectric oligomers to realize magnetic Fano resonances," *ACS Photonics* **2**, 724 (2015).
- ⁸⁰M. I. Tribelsky, J. Geffrin, A. Litman, C. Eyraud, and F. Moreno, "Directional Fano resonances in light scattering by a high refractive index dielectric sphere," *Physical Review B* **94**, 121110 (2016).
- ⁸¹B. Hopkins, A. N. Poddubny, A. E. Miroshnichenko, and Y. S. Kivshar, "Revisiting the physics of Fano resonances for nanoparticle oligomers," *Physical Review A* **88**, 053819 (2013).
- ⁸²L. Carletti, A. Locatelli, D. Neshev, and C. D. Angelis, "Shaping the radiation pattern of second-harmonic generation from AlGaAs dielectric nanoantennas," *ACS Photonics* **3**, 1500 (2016).
- ⁸³R. Camacho-Morales, M. Rahmani, S. Kruk, L. Wang, L. Xu, D. A. Smirnova, A. S. Solntsev, A. Miroshnichenko, H. H. Tan, F. Karouta, S. Naureen, K. Vora, L. Carletti, C. D. Angelis, C. Jagadish, Y. S. Kivshar, and D. N. Neshev, "Nonlinear generation of vector beams from AlGaAs nanoantennas," *Nano Letters* **16**, 7191 (2016).
- ⁸⁴H. Aouani, M. Rahmani, M. Navarro-Cía, and S. A. Maier, "Third-harmonic-upconversion enhancement from a single semiconductor nanoparticle coupled to a plasmonic antenna," *Nature Nanotechnology* **9**, 290 (2014).
- ⁸⁵S. Liu, M. B. Sinclair, T. S. Mahony, Y. C. Jun, S. Campione, J. Ginn, D. A. Bender, J. R. Wendt, J. F. Ihlefeld, P. G. Clem, J. B. Wright, and I. Brener, "Optical magnetic mirrors without metals," *Optica* **1**, 250 (2014).